



Article

Shrinking of Ischia Island (Italy) from Long-Term Geodetic Data: Implications for the Deflation Mechanisms of Resurgent Calderas and Their Relationships with Seismicity

Alessandro Galvani ^{1,*} , Giuseppe Pezzo ¹ , Vincenzo Sepe ¹ and Guido Ventura ^{1,2}

¹ Istituto Nazionale di Geofisica e Vulcanologia, Via di Vigna Murata 605, 00143 Roma, Italy; giuseppe.pezzo@ingv.it (G.P.); vincenzo.sepe@ingv.it (V.S.); guido.ventura@ingv.it (G.V.)

² Istituto per lo Studio degli Impatti Antropici e Sostenibilità in Ambiente Marino, Consiglio Nazionale delle Ricerche (CNR), Capo Granitola (TP), 91021 Campobello di Mazara, Italy

* Correspondence: alessandro.galvani@ingv.it

Abstract: The identification of the mechanisms responsible for the deformation of calderas is of primary importance for our understanding of the dynamics of magmatic systems and the evaluation of volcanic hazards. We analyze twenty years (1997–2018) of geodetic measurements on Ischia Island (Italy), which include the Mt. Epomeo resurgent block, and is affected by hydrothermal manifestations and shallow seismicity. The data from the GPS Network and the leveling route show a constant subsidence with values up to -15 ± 2.0 mm/yr and a centripetal displacement rate with the largest deformations on the southern flank of Mt. Epomeo. The joint inversion of GPS and levelling data is consistent with a 4 km deep source deflating by degassing and magma cooling below the southern flank of Mt. Epomeo. The depth of the source is supported by independent geophysical data. The Ischia deformation field is not related to the instability of the resurgent block or extensive gravity or tectonic processes. The seismicity reflects the dynamics of the shallow hydrothermal system being neither temporally nor spatially related to the deflation.

Keywords: GNSS; velocity field; resurgent caldera; subsidence; earthquakes; degassing processes; modelling



Citation: Galvani, A.; Pezzo, G.; Sepe, V.; Ventura, G. Shrinking of Ischia Island (Italy) from Long-Term Geodetic Data: Implications for the Deflation Mechanisms of Resurgent Calderas and Their Relationships with Seismicity. *Remote Sens.* **2021**, *13*, 4648. <https://doi.org/10.3390/rs13224648>

Academic Editor: João Catalão Fernandes

Received: 28 October 2021

Accepted: 15 November 2021

Published: 18 November 2021

Publisher's Note: MDPI stays neutral with regard to jurisdictional claims in published maps and institutional affiliations.



Copyright: © 2021 by the authors. Licensee MDPI, Basel, Switzerland. This article is an open access article distributed under the terms and conditions of the Creative Commons Attribution (CC BY) license (<https://creativecommons.org/licenses/by/4.0/>).

1. Introduction

The deformation of calderas may be associated with different processes, including the magma accumulation, lateral migration or withdrawal, increase or decrease of gas pressure of hydrothermal systems, and variations in the degassing rate of magma chambers [1]. While uplift phases are indicative of resurgence and may be precursors of volcanic eruptions, testifying to a pressurization of the magmatic system due to magma/gas accumulation or upward magma/fluid migration, subsidence episodes are more difficult to interpret because they may be related to different causes, such as magma cooling and degassing [2], lateral magma migration in sills [3], depressurization of hydrothermal reservoirs [4], regional extension related to tectonics, and gravity instability processes [5]. This is particularly difficult when the subsidence is associated with seismicity. As a result, our understanding of the processes responsible for the subsidence of resurgent calderas represents a primary target to decipher their dynamics. Well-known resurgent calderas include the Campi Flegrei caldera, Italy [6], Yellowstone, USA [7], and Santorini, Greece [8]. All these calderas are characterized by uplift episodes followed by short to long subsidence (deflation) periods with seismicity generally associated with the uplift phases. The identification of the mechanisms responsible for deflation may give us information on the dynamics of the underlying magmatic and hydrothermal systems and on the role of tectonics and gravity processes in modulating the deformation of volcanoes. Aiming to recognize the different causes of the recorded subsidence of Ischia's (Italy) resurgent caldera (Figure 1), we analyze

deformation data from the past twenty years. Ischia Island is located in the northern sector of the Gulf of Naples, Italy, which also includes the Somma-Vesuvius volcano and Campi Flegrei caldera (Figure 1). Nowadays a geodetic GPS survey style network of 22 vertices operates on the island to monitor its deformation behavior [9,10]. The network is managed by INGV—Osservatorio Vesuviano and includes six permanent GPS vertices belonging to INGV—OV and one vertex belonging to the Regione Campania (Figure 2). For the first time, the deformation pattern of the island is investigated by using a GPS dataset from 1997 to 2018. Our analysis also includes leveling data reported by Trasatti et al. (2019) [11]. Results reveal the spatial and temporal displacements; subsequent GPS and levelling data inversion allow us to identify the different causes of measured displacements, revealing the role of passive degassing processes in controlling the deformation of resurgent blocks at calderas. Finally, we discuss the relationships between earthquakes and deformation pattern.

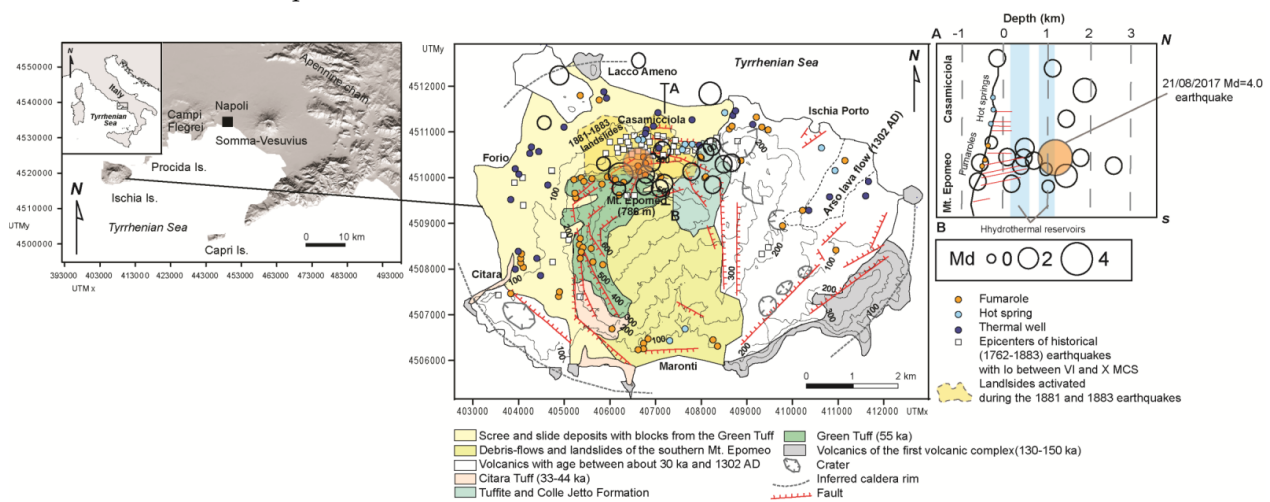


Figure 1. Location and geological map of Ischia Island from [12] with epicentral and hypocentral (N-S cross section) distributions of the 1999–2017 earthquakes from [24]. Historical earthquakes are from [18]. Hydrothermal manifestations are from [17,20]. The depth of the hydrothermal reservoirs in the N-S cross section is from [20,21].

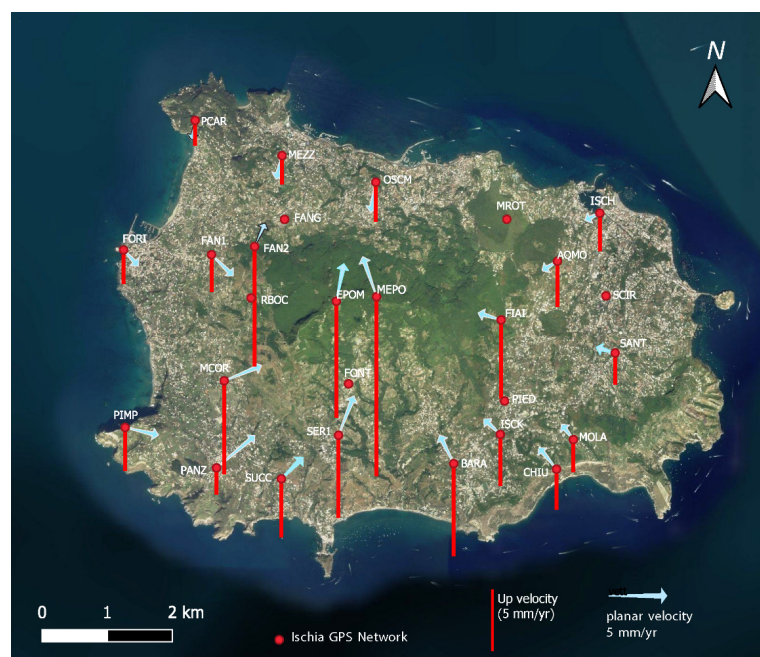


Figure 2. Ischia GPS network and vertical and planar velocity field in mm/yr calculated in the time span 1997–2018.

2. Geological Setting

The volcanism on Ischia occurred between 130–150 ka and 1302 A.D (Figure 1) [12]. The most recent activity (<10 ka) is concentrated in the eastern sector of the island. The resurgent block of Mt. Epomeo (786 m a.s.l.), located in the western sector, uplifted between 55 ka and 19 ka and has been followed by a still active subsidence [13–15]. In the period 1993–2003, measured subsidence rate varies between 1 and 5 mm/year [16,17], and it has been related to fracture closure due to depressurization of the hydrothermal system [17]. The northern flank of Mt. Epomeo is affected by WSW-ESE to E-W striking, north-dipping normal faults (Figure 1), some of which reactivated during the 1883 earthquake (MCS intensity = X) [18,19]. Ischia is also affected by significant hydrothermal activity [20]. A close spatial relationship occurs between the Casamicciola Terme fumaroles, hot springs, and the above-mentioned E-W striking faults (Figure 1). The highest CO₂ (9 t d⁻¹) and steam (135 t d⁻¹) release are measured along the faults that delimit Mt. Epomeo's resurgent structure. Some of these faults are sealed by secondary minerals like gypsum and anhydrite, which are related to the deposition of supersaturated hydrothermal solutions and leaching of the tuffs and lava flows [20,21]. Moreover, a hydrothermal system with heat flow and temperatures up to 40 MW and 250 °C [21], respectively, characterizes the island [22]. The hydrothermal system consists of two sub-horizontal water-vapor reservoirs located at about 400 and 900 m depth with temperatures between 250 and 350 °C and fluid pressures of 4 to 9 MPa, respectively (Figure 1) [20]. These reservoirs are laterally confined by the Mt. Epomeo faults, which, in the Casamicciola Terme area and west of the resurgent block, act as pathways for the rise of hot fluids and gas release (Figure 1). On the basis of resistivity data, the magmatic source responsible for the hydrothermal system heating is supposed to be a laccolith located at depth ≥ 3 km, below Mt. Epomeo [23]. Above the laccolith, subvertical vapor zones cross and feed two hydrothermal reservoirs (Figure 1) [21]. Seismic activity is rather low and generally with low ($M_d < 2$) magnitude events. These events mainly occur along the E-W and NNW-SSE faults delimiting the northern and western sectors of the island where gas emissions and hot water springs also concentrate, and occur within the first 3 km of the crust (Figure 1) [24]. However, the historical record shows that Ischia was struck by some larger magnitude earthquakes, a few of them causing severe damages and fatalities. Remarkable events occurred in 1881 and 1883 in the Casamicciola area and on 21 August 2017, ($M_d = 4$; $M_w 3.9$) [25]. This latter event occurred on the E-W fault system bounding the northern sector of Mt. Epomeo, damaging a limited portion of the Casamicciola area ($I_{\text{max}} = 8$) and causing two fatalities. The 'shallow' source of the $I_0 = X$ 1881, 1883, and $M_d = 4$ 2017 (depth 1.7 km) [26] damaging earthquakes, the 'explosion' in 1995 of a geothermal well drilled between 1940 and 1950, and the occurrence of boiling phreatic aquifers are interpreted to be related to the dynamics of the hydrothermal system [20,25,27], and, in particular, to its pressurization phases. The relevant CLVD component of the focal mechanism of the 21 August, 2017 $M_d = 4$ event, its low frequency character, the low S/P spectral ratio, and the characteristics of the seismic noise also provide evidence of the involvement of pressurized fluids in the source of the Ischia earthquakes [25,26]. The temporal trends of selected geochemical parameters (groundwater discharge temperatures, groundwater Mg/Cl ratios and CO₂ partial pressure) do not show significant variations from 1984 to 2007, suggesting, according to [21], a stable system with a nearly constant thermal and mass transport from depth. As concerns the deformation field, results from SAR data [16] and levelling lines collected in the 1987–2010 [11] and 1990–2003 [17] periods, evidence a subsidence trend, with values up to 1.2 cm/yr centered on the Mt. Epomeo resurgent block, while little or no subsidence occurs on the coastal areas. The observed pattern has been interpreted as due to degassing processes along the faults bounding Mt. Epomeo from a shallow, depressurizing magma reservoir [11,16] or along two main E-W striking, closing cracks corresponding to the Casamicciola fault and the faults bounding the top of Mt. Epomeo [17]. The role of gravity instability processes in controlling the deformation pattern at a local scale has been also recognized (Manzo et al., 2006) [16]. Main processes are the slide of the northwestern sector, activated during the

1881 and 1883 earthquakes, and the rock-fall zones affecting the steep eastern and northern slopes and the summit of Mt. Epomeo (Figure 1).

3. GPS Network and Dataset Processing

Since October 1996, a survey style network of 27 GPS vertices with an inter-distance of 1 to 3 km has been established on Ischia to define the deformation field of the island (Figure 2) [9]. From 1999 to 2013, five of them (AQMO, FORI, OSCM, SANT and SER1) were upgraded into continuous GNSS (CGNSS) stations. The current network configuration also includes the CGNSS station on the top of Mt. Epomeo (MEPO), since March 2017, and one CGNSS station (ISCK) managed by the Campania Region, since 2008 (Figure 2).

The survey style network vertices were realized using 3D-type GPS monuments [9,28]. Siting was performed taking into account the geological and structural features of the island and its urbanization; the benchmarks are located on outcrops or buildings.

During the 1997–2017 time span, all discontinuous stations of the network were repeatedly measured, equipping the GPS stations with TRIMBLE and LEICA receivers and antennas. Each station was occupied for an average observation window ranging from 18 to 24 h for at least 4 survey sessions per station. GPS data were collected at 30 s sampling rate (Table 1).

The complete analyzed dataset, which includes unpublished survey-style data from 2010 to 2017, also considers CGNSS data provided by the CGNSS networks located in the Campania and south Lazio regions. The CGNSS stations belong to different GNSS network providers: the International Global Navigation Satellite Systems GNSS Service IGS [<http://igs.org>, accessed on 26 October 2021, daily available.], the Integrated National GPS Network, RING [29], the Italian Space Agency (Agenzia Spaziale Italiana; ASI) [30], and Leica Geosystems (Italian Positioning Service [ItalPos] network). The CGNSS data cover the period from 1999 to 2018. They are arranged into several clusters, each sharing common fiducial CGNSS stations used as anchor stations in the subsequent combinations. Each cluster was independently processed and then integrated through a least-squares combination into a single daily solution. The GPS observations were processed using the Bernese 5.0 [31] software, based on the Bernese Processing Engine (BPE) procedure, following a standard analysis for regional networks. The daily station coordinates, together with the hourly troposphere parameters, are solved using the a priori Dry Neill troposphere model with the corrections estimated by the Wet Neill mapping function. The ionosphere is neither estimated nor modeled as we used the L3 (ionosphere free) linear combination of L1 and L2. The a priori GPS orbits and the Earth orientation parameters are fixed to the precise IGS products. We applied the ocean-loading finite element solution model FES2004, and used the IGS absolute antenna phase-center corrections. The daily solutions were obtained in a loosely constrained reference frame; i.e., all the a priori station coordinates were left free to 10 m a priori sigma. The time series were obtained by applying minimal inner constraints and a four-parameter Helmert transformation to have the coordinates and errors expressed in the IGS08 reference framework (the IGS realization of the ITRF2008 reference framework). We obtained a velocity field with the estimation of a linear drift (velocity), annual sinusoid, and occasional offsets due to changes in the station equipment in each time series. The formal velocity uncertainties are the white-noise standard deviation multiplied by the variance factors obtained from the time series at each site. We preferred to issue the formal solution without any covariance manipulation, thus focusing on the relative uncertainty between velocities rather than absolute errors.

Table 1. Summary of the geodetic network, velocities, time span acquisition, and number of campaigns.

SITE	East (mm/yr)	sigE (mm/yr)	North (mm/yr)	sigN (mm/yr)	Up (mm/yr)	sigUp (mm/yr)	Tin (initial; yr)	Tfi (final; yr)	# Campaign
AQMO	−1.3185	1.0561	−0.8085	1.0672	−3.7278	0.2328	2001	2018	CGNSS
BARA	−1.2012	1.2281	2.4108	1.4395	−7.6995	5.8372	1998	2017	6
CHIU	−1.5085	0.5462	1.8581	0.6677	−3.2606	2.471	1997	2017	7
EPOM	0.6406	1.138	3.1905	1.3249	−9.8474	4.9739	1997	2017	7
FAN1	1.8555	1.5572	−1.8048	1.6763	−2.9954	7.4253	1998	2017	6
FAN2	0.9177	1.335	2.0247	1.6369	−10.1203	6.5496	1998	2017	6
FIAI	−1.9689	1.3448	0.5986	1.5824	−6.6067	6.636	1999	2017	5
FORI	1.2557	1.0692	−1.3669	1.0853	−2.7434	0.5228	1997	2018	CGNSS
ISCH	−1.2798	1.03	−0.621	1.2643	−3.0754	4.726	1997	2017	7
ISCK	−1.4056	1.057	1.3132	1.1506	−4.2302	0.7274	2008	2018	CGNSS
MCOR	3.1704	1.5771	1.2881	1.6606	−7.7989	7.4588	2003	2017	3
MEPO	−1.1809	1.0394	3.3943	1.1477	−15.1859	5.2276	2017	2018	CGNSS
MEZZ	−0.512	1.199	−2.0104	1.4277	−2.2951	5.6208	1997	2017	7
MOLA	−1.0144	0.9449	1.3155	1.1494	−2.5843	4.4062	1998	2017	7
OSCM	−0.4383	1.0813	−2.5699	1.1087	−3.2291	0.3768	2010	2018	CGNSS
PANZ	3.2801	1.2677	2.7378	1.5565	−2.1145	6.0143	2010	2017	3
PCAR	−0.289	1.2238	−1.6892	1.3691	−1.9985	5.5785	1997	2017	7
PIMP	2.8468	1.3238	−0.6643	1.6352	−3.5494	6.2291	1998	2017	6
SANT	−1.6167	1.1062	0.4773	1.1268	−2.5306	0.4933	2013	2018	CGNSS
SER1	1.3107	0.062	3.3351	0.0748	−6.8572	0.265	2001	2018	CGNSS
SUCC	1.8514	1.2647	1.8193	1.6016	−4.8232	6.0664	1998	2017	7

4. Results

The horizontal velocity field of the complete dataset including southern Lazio region, Campania region with Ponza, Ventotene, and Ischia islands, expressed with respect to a fixed Eurasian plate [32], shows a good coherence with the velocities previously estimated for the Italian peninsula [33,34]. The wide time span of the data set includes the earthquake that struck the island on 21 August 2017. It produced significant offsets only in two continuous GPS stations: MEPO and OSCM (see Figure 3 as an example of time series at OSCM).

The observed displacements were modelled introducing an offset in the respective time series. To better understand the Ischia velocity field, we focused on the island, showing the horizontal velocity field with respect to the island centroid. This latter was obtained by minimizing the horizontal velocities of the GPS stations (Figure 2; Table 1). We also show the vertical velocity field with respect to the reference ellipsoid (Figure 2). The estimated Euler pole and rotation rate for the centroid are at -39.751°N , -165.247°W and $13.5395 \pm 9.974 \text{ deg/Myr}$ in modulus, respectively. Six vertices (FANG, FONT, MROT, PIED, RBOC and SCIR) have been eliminated due to incomplete time series or because they are installed on unstable areas (landslide and rockfall) or have been destroyed. The velocity vectors, reported in Figure 2, converge towards Mt. Epomeo with values ranging from a maximum of 4.27 mm/yr, in the SW, to a minimum of 1.42 mm/yr, in the northern part of the island. The three stations of FAN2, EPOM, and MEPO show patterns deviating from the dominant one. The above-described planar velocity field is accompanied by a general subsidence, ranging from -15.2 mm/yr at Mt. Epomeo to -1.99 mm/yr in the northeastern side of the island. The largest values of subsidence were been observed in the central and southern sectors of Ischia.

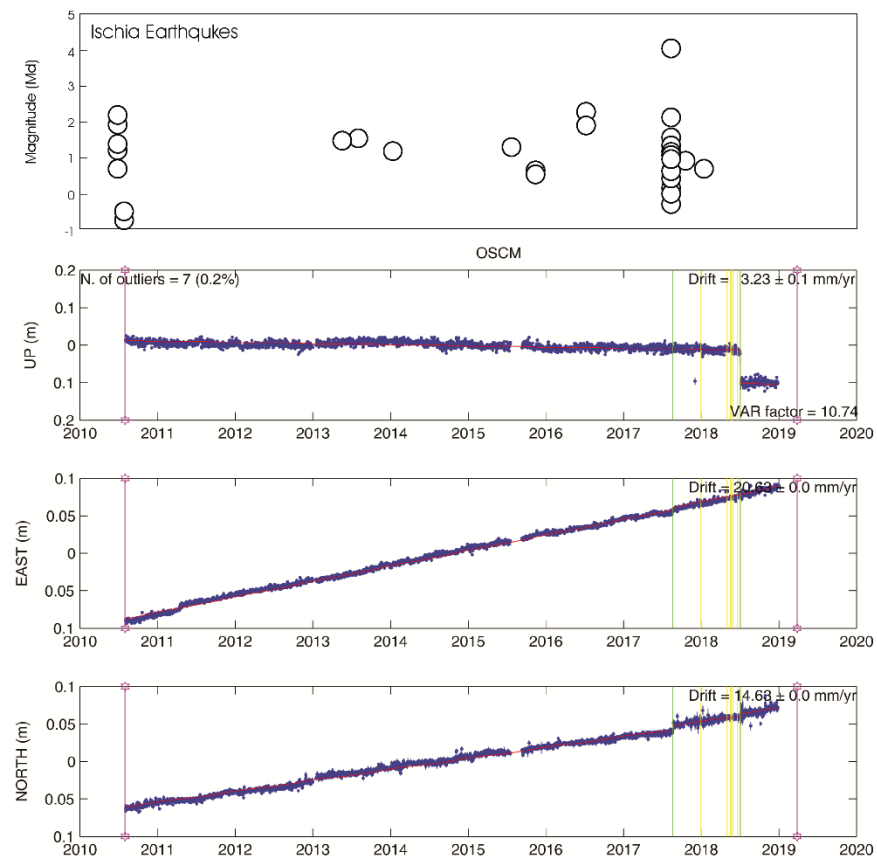


Figure 3. Ischia earthquakes (data from [24]) and OSCM (CGNSS) time series. Violet vertical bars are the starting and ending elaboration times. Yellow bars identify the removal of outlier solutions. Green vertical bar recorded in 2017 testifies of the Md 4 earthquake, whereas the green one recorded in 2018 is due to technical causes.

5. Displacement Field Modelling

In order to identify and characterize the main ground deformation source of Ischia, we performed an analytical modelling by inverting the available ground deformation data. In particular, we used the CGNSS data and the leveling data reported in [11]. Levelling campaigns start from an initial reference point that is assumed to be stable (velocity equal to zero). However, the CGNSS stations close to the leveling reference point measure downwards displacements of about -3 mm/yr. Thus, we calibrated the two datasets, adding to the leveling data a rigid offset of -3.08 mm/yr. To verify the dataset agreement, we compared the leveling velocities at measure points close to the CGNSS benchmarks with CGNSS velocities (see scatter plot in Figure 4). The comparison highlights a good agreement between the two datasets with a correlation index of 0.83. Because Ischia undergoes localized landslide phenomena mainly concentrated in the central and northern sectors of the island [35], we excluded from the modelling some leveling and CGNSS data as specified in the previous section.

To retrieve the source parameters, we jointly inverted the CGNSS and leveling datasets by using an elastic, isotropic, and homogeneous model [36]. We adopt a two-step approach [37] consisting of a non-linear inversion to define the source parameters (north, east, depth, length, width, dip, strike, and homogeneous closing along the plane) by means of a non-linear, least-squares inversion algorithm based on the Levenberg–Marquardt approach. Values of 30 GPa and 0.25 are assumed for the shear modulus and Poisson’s ratio in the half-space, respectively. Because of the complex geological, hydrothermal, and volcanic structural features of Ischia, the deformation source can be assumed to be a horizontal closing layer [21,23,25] whose unknown parameters are the depth, the closing

rate, and spatial extent. During the first step, we defined the source depth, position and homogeneous closing. The parameter uncertainties, best fit and trade-offs (Figure 5) were estimated with 150 restarts of the inversion, adding, each time, a synthetic noise [37].

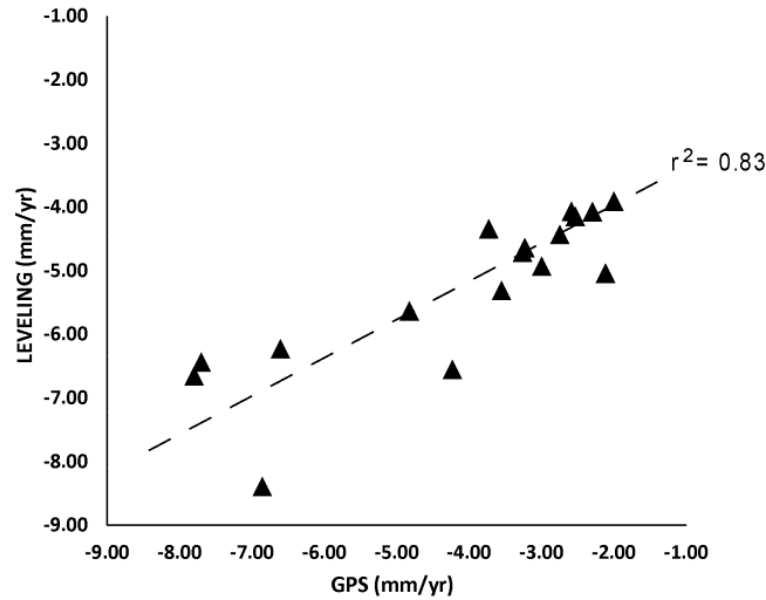


Figure 4. Vertical GPS vs. levelling velocities in mm/yr. The linear regression is reported as a dashed line.

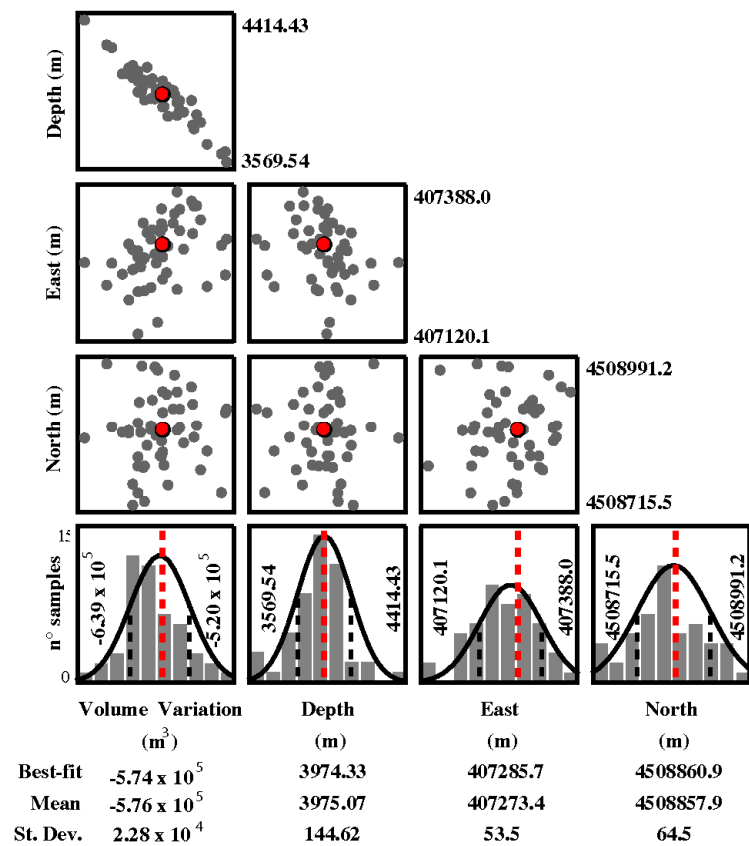


Figure 5. Source depth, position, and volume variation of a homogeneous closing (red symbols). The parameter uncertainties, best fit (in red), and trade-offs are shown.

The best-fit model reveals a horizontal closing crack at about 4 km depth located below the southern flank of Mt. Epomeo. The depth value appears different from the 2 km obtained by [11], whose inversion includes only levelling data. Although the non-linear inversion concentrates best solutions around 4 km depth, during the second step, we took into account both 2 km and 4 km depth results, and performed a ground velocity linear inversion exploring both solutions. Source closing distributions, and observed, modeled, and the residual (observed minus modelled) velocities from both linear inversions are reported in Figure 6. Closing distribution is calculated as closing rate (mm/yr) on a 0.5×0.5 km grid along the horizontal plane. The resulting closing rate corresponds to $-3.66 \times 10^5 \text{ m}^3/\text{yr}$ and $-3.19 \times 10^5 \text{ m}^3/\text{yr}$ for 4 and 2 km depth models, respectively (Table 2). Both models well reproduce the quasi-centripetal horizontal velocity pattern and the concentric vertical one. However, the 2 km depth model underestimates the central subsidence pattern of leveling data (Panel j in Figure 6), the horizontal CGNSS centripetal pattern (Panel a in Figure 6), and overestimates the vertical CGNSS components (Panel b in Figure 6). Therefore, we favor the 4 km depth model, with the source of deformation located in the southern sector of Mt. Epomeo.

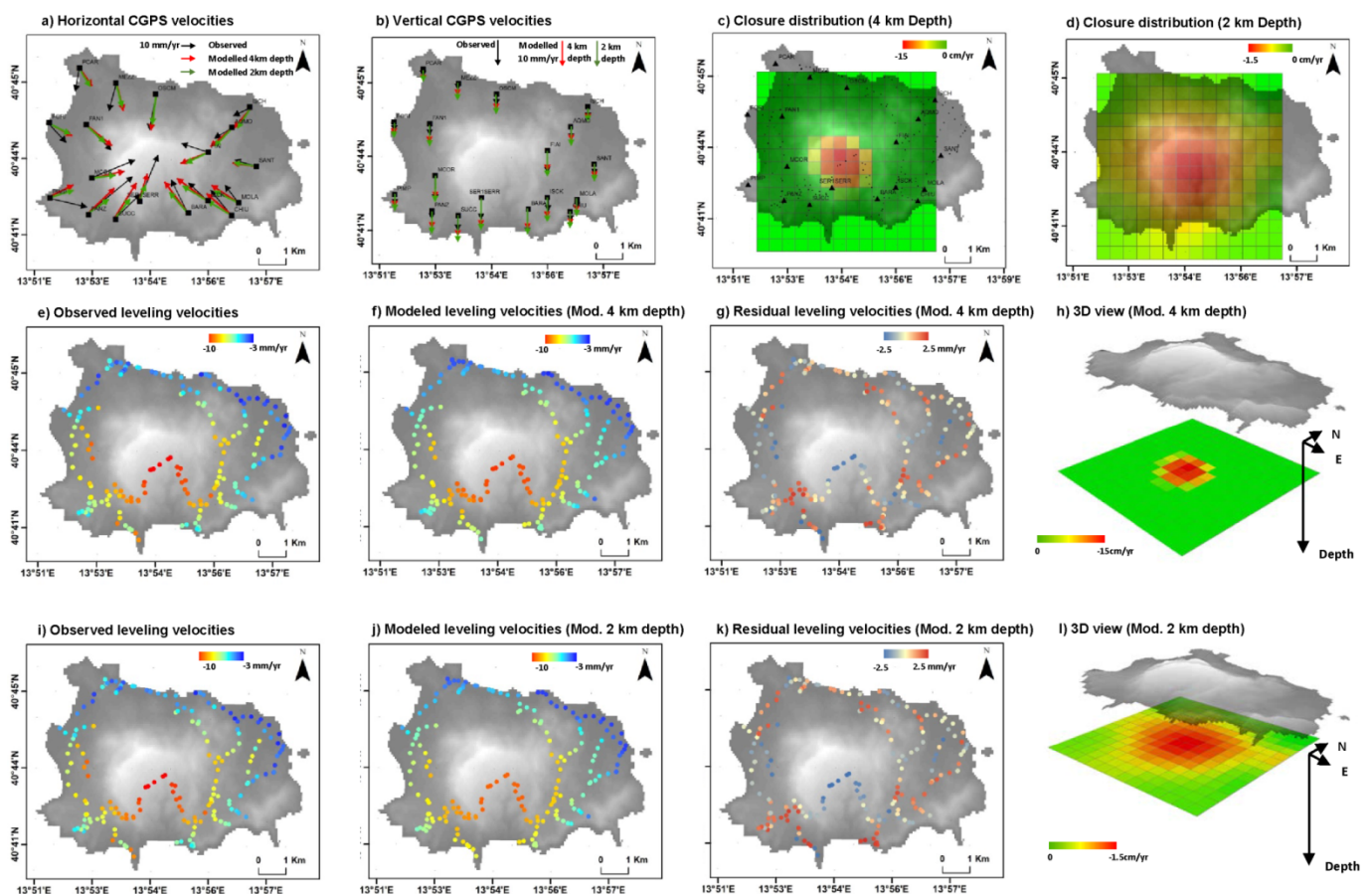


Figure 6. (a) Horizontal and (b) vertical GNSS velocities on Ischia Island. Black arrows represent the observed vectors; red and green ones are the modelled velocities for 4 km and 2 km depth models respectively; in (c,d), the corresponding closing distributions for both models. Panels in second and third rows (e–k), report the observed, modelled, and residual levelling velocities for 4 km and 2 km depth models respectively; in panel (h,l) the corresponding 3D views of both displacement models are shown.

Table 2. Parameters of the retrieved deformation sources (depth, mesh, and mean volume).

Model	Mesh (m)	Mean Δ Volume (m ³)
2 km Depth	7000 × 7000	−319,225
4 km Depth	7000 × 7000	−366,325

6. Discussion

The 1997–2017 GNSS and leveling data show that Ischia is mainly characterized by a deformation field recording a general contraction, a feature observed in other volcanic areas, e.g., at Dallol and Askja [38,39], among others. At Ischia, this is testified by the general subsidence and a centripetal pattern of the horizontal deformation field, with maximum velocities, in both horizontal and vertical components, recorded in the Mt. Epomeo area. Only a few GPS stations diverge from the centripetal pattern, because of gravity instability phenomena [35]. The deformation rate remains nearly constant at each station and neither horizontal and vertical deformations showed significant changes in their rate after the $M_d = 4$, 21 August 2017 earthquake (Figures 1 and 3). According to Calderoni et al. (2019) [25], the Ischia earthquakes are associated with hydrothermal pressurization processes and degassing and not with tectonics or the Mt. Epomeo subsidence. Taking also into account that historical and instrumental earthquakes concentrate in the northern sector of the island, we realistically conclude that the long term deformation field is due neither to earthquake dynamics nor to gravity processes. This latter conclusion is also consistent with the lack of relationships between topography and deformation rate. We also exclude the possibility that the recorded deformation field is due to the closure of two subvertical, E-W striking cracks located in the southern and northern sectors of Mt. Epomeo, as proposed by [17], because the recorded centripetal pattern of the deformation is not consistent with this geometry of sources. Moreover, the lack of significant changes in the chemical compositions of the gas and hot water emissions [21] and of uplift phases exclude the possible emplacement of magma and, possibly, of its lateral migration at depth. Therefore, the recorded contraction could be related to the huge degassing [20] and cooling, possibly reflecting crystallization of a magma reservoir, as also suggested by Trasatti et al. (2019) [11] on the basis of levelling data and coupled geochemical–deformation models. The results of our modeling of the combined GPS and levelling data at Ischia indicate two possible solutions: a sill-like source located at 2 km or 4 km depth. The occurrence of a sill at a depth of 4 km fits the observed pattern of vertical and horizontal deformation better. In addition, available resistivity data [23] indicate a high resistivity body extending from the surface to a depth of at least 3 km below Mt. Epomeo and the Ischia earthquakes are confined within the upper 3 km of the crust [24]. Moreover, the rheological model proposed by Castaldo et al. [40] shows a dome-like elasto-plastic transition in which the main magmatic body lies below a depth of 3 km. Our data indicate that this sill is located below the southern flank of Mt. Epomeo, in an area not affected by earthquakes. In addition, the nearly constant subsidence of the resurgent block does not re-activate its eastern and western bounding faults. Therefore, the deflation dynamics of such a sill does not explain the seismicity of the island. The only seismically active structures on Ischia are represented by E-W striking faults located at the base of the northern flank of the resurgence block, which are frequently re-activated by earthquakes [18,41]. Indeed, most earthquakes occur in areas where fumaroles and hot water emissions concentrate, i.e., in the Casamicciola area (Figure 1). In this framework, the cooling magma at a depth of 4 km releases fluids which mainly expand laterally from the sill, because the rocks overlying the sill include the impermeable ‘Green Tuff’: hydrothermally altered tuffs and lava flows with sealed fractures [40]. These fluids feed the two hydrothermal reservoirs located at about 1 km and 400 m depth [21] and upraise to the surface along the E-W striking fault of the northern flank of Mt. Epomeo and, to a lesser extent, at the northern tip of the eastern NNW-SSE striking, Mt. Epomeo bounding faults. The upraise and pressurization of these fluids within the hydrothermal reservoirs may trigger seismicity, which, at least for the

August Md 4 event, is very shallow (1.7 km depth) [25]. The above-reported conceptual model is summarized in Figure 7.

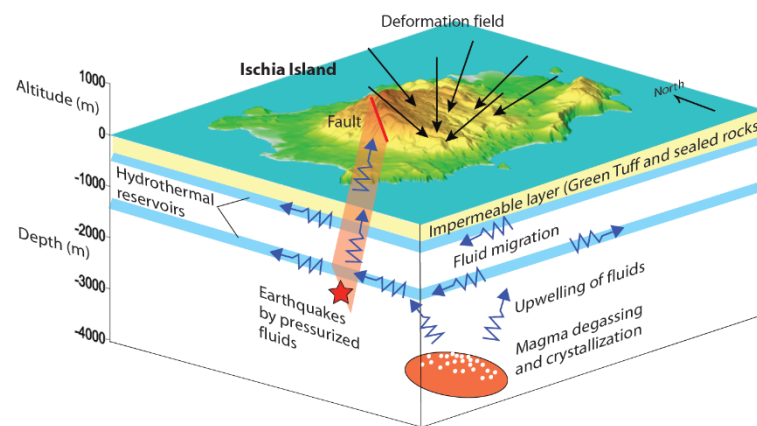


Figure 7. Sketch summarizing the conceptual model of the dynamics of Ischia Island and in particular the relationship among magma degassing, seismicity, and deformation.

Our data show that the eastern sector of Ischia, where the volcanic activity <30 ka concentrated, is characterized by the lower values of subsidence and horizontal deformation, this latter consistent with the above described centripetal arrangement (Figure 2). This indicates that this sector of the island is ‘inactive’, at least from a deformation point of view. Taking into account that only few hydrothermal manifestations and no earthquakes characterizes the eastern sector, we suggest that (a) dynamic processes related to possible magma or hydrothermal activity at depth are virtually lacking in this sector and (b) the most active sector of the island is the western one, where the inferred source of deformation has been identified and modeled, and where hydrothermal manifestations and earthquakes concentrate. In this framework, the possible signs of reactivation of the Ischia magmatic system are expected to include a decrease in the subsidence rate or an uplift, a centrifugal pattern of the horizontal deformation, a deformation pattern of the eastern sector of the island not compatible with a source located below Mt. Epomeo.

7. Conclusions

The main conclusions of this study may be summarized in the following points:

- (a) Ischia is characterized by a 1997–2017 deformation pattern indicating subsidence and contraction of its western sector.
- (b) The observed pattern is consistent with a deflating and contracting sill-like source located at 4 km depth. The sill is affected by cooling and degassing processes.
- (c) The recorded deformations are not compatible with the seismicity of the island, which is mainly associated with the dynamics of the hydrothermal system and not with that of the deflating sill.
- (d) A change in the rate of the recorded 1997–2017 deformation in the western sector of the island and/or the occurrence of a deformation pattern compatible with a source located in the eastern sector could be signs of the reactivation of the Ischia magmatic system.

Our results provide evidence that the subsidence of resurgent calderas may be associated with the deflation of a residual magma reservoir and that a decoupling between the dynamics of a magma reservoir, in this case, deflation, and of the overlying hydrothermal system may occur. In addition, we highlight that in quiescent calderas, the seismicity may not be related to the deformation pattern induced by magmatic processes.

Author Contributions: Conceptualization, A.G., G.P., G.V.; data collection, V.S.; methodology, A.G., G.P.; software, A.G., G.P.; validation, G.V.; writing—original draft preparation, A.G., G.P., G.V.; writing-review and editing, A.G., G.P., G.V.; visualization, A.G., G.P., G.V.; supervision, A.G., G.P., G.V.; project administration, V.S. All authors have read and agreed to the published version of the manuscript.

Funding: The present work is supported by INGV.

Institutional Review Board Statement: Not applicable.

Informed Consent Statement: Not applicable.

Data Availability Statement: The data presented in this study are available on request from the corresponding author.

Acknowledgments: We are very grateful to Roberto Devoti and Grazia Pietrantonio and Simone Atzori for supporting and data modelling for discussions and computational support.

Conflicts of Interest: The authors declare no conflict of interest. The funders had no role in the design of the study; in the collection, analyses, or interpretation of data; in the writing of the manuscript, or in the decision to publish the results.

References

- Lowenstern, J.B.; Smith, R.B.; Hill, D.P. Monitoring super-volcanoes: Geophysical and geochemical signals at Yellowstone and other large caldera systems. *Philos. Trans. Royal Soc. A* **2006**, *364*, 2055–2072. [[CrossRef](#)] [[PubMed](#)]
- Caricchi, L.; Biggs, J.; Annen, C.; Ebmeier, S. The influence of cooling, crystallisation and re-melting on the interpretation of geodetic signals in volcanic systems. *Earth Planet. Sci. Lett.* **2014**, *388*, 166–174. [[CrossRef](#)]
- Macedonio, G.; Giudicepietro, F.; D’Auria, L.; Martini, M. Sill intrusion as a source mechanism of unrest at volcanic calderas. *J. Geophys. Res. Solid Earth* **2014**, *119*, 3986–4000. [[CrossRef](#)]
- Kwoun, O.I.; Lu, Z.; Neal, C.; Wicks, C. Quiescent deformation of the Aniakchak Caldera, Alaska, mapped by InSAR. *Geology* **2006**, *34*, 5–8. [[CrossRef](#)]
- Newhall, C.G.; Dzurisin, D. Historical Unrest at large calderas of the world. *US Geol. Survey Bull.* **1988**, *1855*, 1–27.
- Trasatti, E.; Polcari, M.; Bonafede, M.; Stramondo, S. Geodetic constraints to the source mechanism of the 2011–2013 unrest at Campi Flegrei (Italy) caldera. *Geophys. Res. Lett.* **2015**, *42*, 3847–3854. [[CrossRef](#)]
- Chang, W.L.; Smith, R.B.; Farrell, J.; Puskas, C.M. An extraordinary episode of Yellowstone caldera uplift, 2004–2010, from GPS and InSAR observations. *Geophys. Res. Lett.* **2010**, *37*, L23302. [[CrossRef](#)]
- Foumelis, M.; Trasatti, E.; Papageorgiou, E.; Stramondo, S.; Parcharidis, I. Monitoring Santorini volcano (Greece) breathing from space. *Geophys. J. Inter.* **2013**, *193*, 161–170. [[CrossRef](#)]
- De Martino, P.; Tammara, U.; Obrizzo, F.; Sepe, V.; Brandi, G.; D’Alessandro, A.; Pingue, F. The GPS network of Ischia Island: Ground deformations in an active volcanic area (1998–2010). *Quad. Geofis.* **2011**, *95*, 95.
- Tammara, U.; De Martino, P.; Obrizzo, F.; Brandi, G.; D’Alessandro, A.; Dolce, M.; Malaspina, S.; Serio, C.; Pingue, F. Somma Vesuvius volcano: Ground deformations from CGPS observations (2001–2012). *Ann. Geophys.* **2013**, *56*, S0456. [[CrossRef](#)]
- Trasatti, E.; Acocella, V.; Di Vito, M.A.; Del Gaudio, C.; Weber, G.; Aquino, I. Magma degassing as a source of long-term seismicity at volcanoes: The Ischia island (Italy) case. *Geophys. Res. Lett.* **2019**, *46*, 14421–14429. [[CrossRef](#)]
- Vezzoli, L. Island of Ischia, *Quad. Ric. Sci.* **1988**, *114*, 133.
- Civetta, L.; Gallo, G.; Orsi, G. Sr- and Nd-isotope and trace-element constraints on the chemical evolution of the magmatic system of Ischia (Italy) in the last 55 ka. *J. Volcanol. Geotherm. Res.* **1991**, *46*, 213–230. [[CrossRef](#)]
- Gillot, P.-Y.; Chiesa, S.; Pasquaré, G.; Vezzoli, L. 33,000-yr K–Ar dating of the volcano–tectonic horst of the Isle of Ischia, Gulf of Naples. *Nature* **1982**, *299*, 242–245. [[CrossRef](#)]
- Sbrana, A.; Toccaceli, R.M.; Biagio, G.; Cubellis, E.; Faccenna, C.; Fedi, M. *Carta Geologica n. 464 Isola di Ischia Scala 1:10.000- Cartografia e Note Illustrative*; Regione Campania: Napoli, Italy, 2011.
- Manzo, M.; Ricciardi, G.P.; Casu, F.; Ventura, G.; Zeni, G.; Borgström, S. Surface deformation analysis in the Ischia Island (Italy) based on spaceborne radar interferometry. *J. Volcanol. Geotherm. Res.* **2006**, *151*, 399–416. [[CrossRef](#)]
- Sepe, V.; Atzori, S.; Ventura, G. Subsidence due to crack closure and depressurization of hydrothermal systems: A case study from Mt Epomeo (Ischia Island, Italy). *Terra Nova* **2007**, *19*, 127–132. [[CrossRef](#)]
- Alessio, G.; Esposito, E.; Ferranti, L.; Mastrolorenzo, G.; Porfido, S. Correlazione tra sismicità ed elementi strutturali nell’isola d’Ischia. *Il Quat.* **1996**, *9*, 303–308.
- Tibaldi, A.; Vezzoli, L. A new type of volcano flank failure: The resurgent caldera sector collapse, Ischia, Italy. *Geophys. Res. Lett.* **2004**, *31*, L14605. [[CrossRef](#)]
- Chiodini, G.; Avino, R.; Brombach, T.; Caliro, S.; Cardellini, C.; De Vita, S. Fumarolic and diffuse soil degassing west of Mount Epomeo, Ischia, Italy. *J. Volcanol. Geotherm. Res.* **2004**, *133*, 291–309. [[CrossRef](#)]

21. Di Napoli, R.; Aiuppa, A.; Bellomo, S.; Brusca, L.; D'Alessandro, W.; Candela, E.G. A model for Ischia hydrothermal system: Evidences from the chemistry of thermal groundwaters. *J. Volcanol. Geotherm. Res.* **2009**, *186*, 133–159. [[CrossRef](#)]
22. Panichi, C.; Bolognesi, L.; Ghiara, M.R.; Noto, P.; Stanzione, D. Geothermal assessment of the island of Ischia (southern Italy) from isotopic and chemical composition of the delivered fluids. *J. Volcanol. Geotherm. Res.* **1992**, *49*, 329–348. [[CrossRef](#)]
23. Di Giuseppe, M.G.; Troiano, A.; Carlino, S. Magnetotelluric imaging of the resurgent caldera on the island of Ischia (southern Italy): Inferences for its structure and activity. *Bull. Volcanol.* **2017**, *79*, 85. [[CrossRef](#)]
24. D'Auria, L.; Giudicepietro, F.; Tramelli, A.; Ricciolino, P.; Bascio, D.L.; Orazi, M. The seismicity of Ischia Island. *Seism. Res. Lett.* **2018**, *89*, 1750–1760. [[CrossRef](#)]
25. Calderoni, G.; Di Giovambattista, R.; Pezzo, G.; Albano, M.; Atzori, S.; Tolomei, C.; Ventura, G. Seismic and geodetic evidences of a hydrothermal source in the Md 4.0, 2017, Ischia earthquake (Italy). *J. Geophys. Res. Solid Earth* **2019**, *124*, 5014–5029. [[CrossRef](#)]
26. Braun, T.; Famiani, D.; Cesca, S. Seismological constraints on the source mechanism of the damaging seismic event of 21 August 2017 on Ischia Island (Southern Italy). *Seism. Res. Lett.* **2018**, *89*, 1741–1749. [[CrossRef](#)]
27. Cubellis, E.; Luongo, G. *Il terremoto del 28 luglio 1883 a Casamicciola nell'isola d'Ischia—“Il contesto fisico” Monografia n.1, Presidenza del Consiglio dei Ministri; Servizio Sismico Nazionale, Istituto Poligrafico e Zecca dello Stato: Roma, Italy, 1998; pp. 49–123.*
28. Anzidei, M.; Baldi, P.; Pesci, A.; Del Mese, S.; Esposito, A.; Galvani, A.; Loddo, F.; Massucci, A.; Cristofolletti, P. La rete geodetica dell'appennino centrale CA- GeoNet. *Quad. Geofis.* **2008**, *54*, 1–41.
29. Avallone, A.; Selvaggi, G.; D'Anastasio, E.; D'Agostino, N.; Pietrantonio, G.; Riguzzi, F.; Serpelloni, E.; Anzidei, M.; Casula, G.; Cecere, G.; et al. The RING network: Improvement of a GPS velocity field in the central Mediterranean. *Ann. Geophys.* **2010**, *53*, 39–54. [[CrossRef](#)]
30. Vespe, F.; Bianco, G.; Fermi, M.; Ferraro, C.; Nardi, A.; Sciarretta, C. The Italian GPS fiducial network: Services and products. *J. Geodyn.* **2000**, *30*, 327–336. [[CrossRef](#)]
31. Beutler, G.; Bock, H.; Dach, R.; Fridez, P.; Gäde, A.; Hugentobler, U.P.; Jäggi, A.; Meindl, M.; Mervart, L.; Prange, L.; et al. *Bernese GPS Software Version 5.0*; Dach, R., Hugentobler, U., Fridez, P., Meindl, M., Eds.; Astronomical Institute, University of Bern: Bern, Switzerland, January 2007.
32. Altamimi, Z.; Métivier, L.; Collilieux, X. ITRF2008 plate motion model. *J. Geophys. Res. Solid Earth* **2012**, *117*, B07402. [[CrossRef](#)]
33. Devoti, R.; D'Agostino, N.; Serpelloni, E.; Pietrantonio, G.; Riguzzi, F.; Avallone, A.; Cavaliere, A.; Cheloni, D.; Cecere, G.; D'Ambrosio, C.; et al. A Combined Velocity Field of the Mediterranean Region. *Ann. Geophys.* **2017**, *60*, S0215. [[CrossRef](#)]
34. Devoti, R.; Riguzzi, F. The velocity field of the Italian area. *Rend. Fis. Acc. Lincei* **2018**, *29*, 51–58. [[CrossRef](#)]
35. Della Seta, M.; Marotta, E.; Orsi, G.; de Vita, S.; Sansivero, F.; Fredi, P. Slope instability induced by volcano-tectonics as an additional source of hazard in active volcanic areas: The case of Ischia island (Italy). *Bull. Volcanol.* **2012**, *74*, 79–106. [[CrossRef](#)]
36. Okada, Y. Surface deformation due to shear and tensile faults in a half-space. *Bull. Seismol. Soc. Am.* **1985**, *75*, 1135–1154. [[CrossRef](#)]
37. Atzori, S.; Manunta, M.; Fornaro, G.; Ganas, A.; Salvi, S. Postseismic displacement of the 1999 Athens earthquake retrieved by the Differential Interferometry by Synthetic Aperture Radartime series. *J. Geophys. Res. Solid Earth* **2008**, *113*, B09309. [[CrossRef](#)]
38. Battaglia, M.; Pagli, C.; Meuti, S. The 2008–2010 Subsidence of Dallol Volcano on the Spreading Erta Ale Ridge: InSAR Observations and Source Models. *Remote Sens.* **2021**, *13*, 1991. [[CrossRef](#)]
39. de Zeeuw-van Dalfsen, E.; Pedersen, R.; Hooper, A.; Sigmundsson, F. Subsidence of Askja caldera 2000–2009: Modelling of deformation processes at an extensional plate boundary, constrained by time series InSAR analysis. *J. Volcanol. Geotherm. Res.* **2021**, *213*, 72–82. [[CrossRef](#)]
40. Castaldo, R.; Gola, G.; Santilano, A.; De Novellis, V.; Pepe, S.; Manzo, M.; Tizzani, P. The role of thermo-rheological properties of the crust beneath Ischia Island (Southern Italy) in the modulation of the ground deformation pattern. *J. Volcanol. Geotherm. Res.* **2017**, *344*, 154–173. [[CrossRef](#)]
41. Sbrana, A.; Marianelli, P.; Pasquini, G. Volcanology of Ischia (Italy). *J. Maps* **2018**, *14*, 494–503. [[CrossRef](#)]